

Analysis of Dynamic Optical Imaging Data

B. Pesaran^{1,*}, A. T. Sornborger², N. Nishimura³, D. Kleinfeld³ and P. P. Mitra⁴

1. Department of Biology

Caltech, 216-76

Pasadena, CA 91125

bijan@caltech.edu

Tel: (626) 395 8337

Fax: (626) 795 2397

2. Departments of Mathematics and Engineering

University of Georgia

Athens, GA 30602

ats@camelot.mssm.edu

Tel: (212) 241 4033

Fax: (212) 426 5037

3. Department of Physics

University of California at San Diego

La Jolla, CA 92093-0319

nnishimura@physics.ucsd.edu

dk@physics.ucsd.edu

Tel: (858) 534 3562

Fax: (858) 534 7697

4. Freeman Bldg.

Cold Spring Harbor Laboratory

1 Bungtown Road

Cold Spring Harbor, NY 11724

pmitra@bell-labs.com

Tel: (516) 367 8457

Fax: (516) 367 8389

*: Corresponding author.

Goal

Dynamic optical imaging experiments generate large, multivariate data sets that contain signal and noise components of considerable spatio-temporal complexity. Advances in available computational power now make it possible to identify and remove noise components and characterize signal structure in a timely manner through the use of modern signal and image processing techniques. The goal of this chapter is to present these techniques and illustrate their application to the analysis of optical imaging data.

Area of application

Noise in imaging data arises from two broad categories of sources, biological and technical. Biological sources like cardiac and respiratory cycles are routinely present, as well as motion of the experimental subject and slow vasomotor oscillations (Mayhew et al., 1996; Mitra et al., 1997; Kalatsky and Stryker, 2003). In all studies of evoked activity, ongoing brain activity not locked to or triggered by the stimulus is another source of biological noise. Technical noise sources in imaging experiments include photon counting statistics, electronic instrumentation, 50/60 Hz electrical activity, CCD camera refresh rates, and building vibrations to name a few. All of this activity combines to mask the neuronal signals of interest.

This chapter presents signal and image processing techniques that have proven to be useful in the analysis of optical imaging. The main techniques are drawn from multitaper spectral analysis, harmonic analysis and the singular value decomposition (SVD). The tools will be illustrated on two data sets: optical imaging data from rat primary somatosensory cortex and cat primary visual cortex.

The spectral methods presented here play a central role to sort out physiological artifacts and stimulus response with trial-averaging. While the procedures overlap to a certain degree, the removal of physiological artifacts makes use of the harmonic analysis method, while stimulus response characterization uses the periodic stacking method.

Application area	Method
Removal of physiological artifacts	Harmonic analysis
Stimulus response with trial averaging	Periodic stacking method

Mathematical methods

Four tools for the analysis of optical imaging data are presented below; multitaper spectral estimation, harmonic analysis, the SVD in two different forms and the periodic stacking method. This presentation is focused on the use of the tools rather than on their derivation. Further information on the technical aspects of the discussion is available in (Thomson, 1982; Percival and Walden, 1993; Mitra and Pesaran, 1999; Sornborger et al., 2003a). With regard to the choice of software, we typically do calculations in MATLAB

(Mathworks, MA), a general purpose language for numerical analysis and visualization. MATLAB has a routine to calculate the Slepian functions used in spectral analysis called **dpss**. MATLAB also has a routine to calculate fast Fourier transforms called **fft** and a routine to calculate singular value decompositions called **svd**. In the statistics toolbox, one finds a routine to calculate the cumulative and inverse F-distribution functions called **fcdf** and **finv**, respectively. In the signal processing toolbox, there is a routine for calculating a multitaper power spectrum estimate called **pmtm**. All of these routines are helpful for coding the methods outlined below.

Multitaper Spectral Estimation

Spectral estimation is based on the premise that the frequency domain is the appropriate basis in which to examine dynamic activity. This assumes that the activity is stationary. While this is not usually true of neural activity on long time-scales, say hours, it is not unreasonable to suggest that on a sub-second time-scale neural processes change very little. The approach is to then repeat the calculation on neighboring windows overlapping in time, usually displaced by a fixed amount. The result, called the spectrogram, is a time-frequency representation of the function being calculated.

Conventional spectral analysis involves multiplying time series data by a single time series of the same length known as a taper, or more conventionally as a window function. Examples of such single tapers are Hamming, Hanning and Cosine tapers. We use multitaper methods in which many tapers are used to operate on a single window in time of the data. The tapers used are the Slepian functions, or discrete prolate spheroidal sequences (DPSS), which form a set of orthogonal functions. The Slepian functions are characterized by a single parameter, W , also called the bandwidth parameter. This parameter specifies the frequency and bandwidth of the Slepian functions. For a given frequency half-bandwidth W and length N , there are approximately $2NW$ Slepian functions $w_t(k)$ ($k = 1, \dots, \lfloor 2NW \rfloor$, $t = 1, \dots, N$) that have their power concentrated in the frequency range $[-W, W]$.

Step 1: Computing the Slepian functions

The Slepian functions are characterized by their length, N , and bandwidth parameter, W . The parameters N and W determine the maximum number of functions useable, $K = \lfloor 2NW \rfloor$ and their selection is up to the judgment of the investigator based on a knowledge of the dynamics of the processes under investigation. This choice is then best made iteratively by visual inspection and some degree of trial and error. $2NW$ gives the number of effectively independent frequencies over which the spectral estimate is effectively smoothed, so that the variance in the estimate is typically reduced by a factor $2NW$. Thus, the choice of $2W$ is a choice of how much to smooth. As a rule of thumb we find that fixing the time bandwidth product NW at a small number (typically 3 or 4) and then varying the window length in time until sufficient spectral resolution is obtained is a reasonable strategy.

Step 2: Computing the tapered Fourier transforms

The next step is the computation of the tapered Fourier transforms of the data x_t ($t = 1, \dots, N$), for each taper $w_t(k)$ ($k = 1, \dots, K$)

$$\tilde{x}_k(f) = \sum_{t=1}^N w_t(k) x_t \exp(-2\pi i f t) \quad \text{Equation 1}$$

It is important to note before taking the tapered Fourier transform, the data is typically padded with zeros (Mitra and Pesaran, 1999) to the nearest power of 2 greater than γN where γ is an integer greater than 2. The zeros are added to one end of the time series after they are multiplied by the tapers.

Step 3: Direct spectral estimate

The simplest example of the multitaper method is the direct multitaper spectral estimate, $S_{MT}(f)$ which is simply the average over individual tapered spectral estimates,

$$S_{MT}(f) = \frac{1}{K} \sum_{k=1}^K |\tilde{x}_k(f)|^2 \quad \text{Equation 2}$$

The spectrum may be computed with a moving window to obtain a spectrogram which provides a time-frequency representation of the data.

Harmonic analysis

Multitaper methods provide a robust and efficient way to carry out harmonic analysis: the analysis of discrete sinusoidal components of activity present in a continuous background. This allows the detection, estimation of parameters and extraction of the sinusoidal activity on a short moving window.

An optimally sized analysis window is needed. This window must be sufficiently small to capture the variations in the amplitude, frequency, and phase, but long enough to have the frequency resolution to separate the relevant peaks in the spectrum, both artifactual and originating in the desired signal.

Step 1: Detection and estimation of a sinusoid in a colored background

The presence of a sinusoidal component in colored noise background may be detected by a test based on a goodness of fit F-statistic (Thomson, 1982). The activity is modeled a sinusoid of frequency, f , with a certain amplitude and phase added to a random noise process that is locally white on a scale given by the bandwidth parameter W of the tapers.

$$a(t) = \sum_n A_n \cos[f_n t + \phi_n] + \delta a(t) \quad \text{Equation 3}$$

The amplitude, A_n , and phase, ϕ_n , are given by the complex amplitude, $\mu_n(f_n)$, of the cosine wave. This complex amplitude can be estimated using the tapered Fourier transforms of the data, $x_k(f)$, and the Fourier transform of the tapers themselves at zero frequency, $U_k(0)$. For this application, we find that the data should be padded by a factor of at least 25, and we usually pad by a factor of 100.

$$\begin{aligned} \mu_n(f_n) &= \frac{A_n}{2} \exp(i\phi_n) \\ \hat{\mu}_n(f_n) &= \frac{\sum_k \tilde{x}_k(f_n) U_k(0)}{\sum_k |U_k(0)|^2} \end{aligned} \quad \text{Equation 4}$$

The goodness of fit F-statistic, which allows us to test the hypothesis that the sine wave is present at that frequency, is given by

$$F(f_n) = \frac{(K-1) |\hat{\mu}_n(f_n)|^2 \sum_k |U_k(0)|^2}{\sum_k |\tilde{x}_k(f_n) - \hat{\mu}_n(f_n) U_k(0)|^2} \quad \text{Equation 5}$$

The quantity in Equation 5 is F-distributed with $(2, 2K-2)$ degrees of freedom. The significance level is chosen to be $1 - 1/N$ so that on average there will be one false detection of a sinusoid across all frequencies.

If the cause of the estimated sinusoid is considered to be noise, as may occur from regular breathing, heart beat or electrical noise, one may subtract it from the data and the spectrum of the residual time series may be obtained as before.

Step 2: Removal of periodic components

Sometimes the parameters of periodic components vary slowly in time, drifting in center frequency, amplitude, or phase. The parameters A_n , f_n , and ϕ_n can be estimated as a function of time by using a moving time window. The goal is to estimate the smooth functions $A_n(t)$, $f_n(t)$, and $\phi_n(t)$ to give the component to be subtracted from the original time series.

The frequency F-test described above is used to determine the fundamental frequency tracks $f_n(t)$ in Equation 3. The time series used for this purpose may either be a single time series in the data or an independently monitored physiological time series. The sequence of the fundamental frequency over time is then used to construct the frequencies for the harmonics and sums and differences of individual oscillations, usually respiration and cardiac rhythms, generated by interactions between them. The final set $f_n(t)$ contains all these frequencies.

The estimated sinusoids are reconstructed for each analysis window, and the successive estimates are overlap-added to provide the final model waveform for the artifacts. If more precision is required, the estimates for the amplitude and phase for each window can be interpolated to each digitization point to allow for nonlinear phase changes over the shift between each window. This is akin to using a shift in time between two successive analysis windows of the sampling rate but achieved at far less computational cost.

More details on implementation of this procedure are given below in the Protocol and procedures and Example of application sections.

Multivariate time series methods

To this point in the presentation, the operations have been described on univariate data, but optical imaging experiments record many pixels of activity simultaneously which leads to multivariate time series.

The SVD is a general matrix decomposition of fundamental importance that is equivalent to principal component analysis in multivariate statistics, and generates low dimensional representations for complex multidimensional time series. These low-dimensional representations are formed from distinct modes that are orthogonal to each other. Consequently, the SVD is a powerful tool to reduce the number of interesting dimensions of the data and to characterize coherent states of activity. Here, we present two applications of the SVD, one to imaging data in its more usual space and time dimensions, the space-time SVD, and one when we have Fourier transformed the time dimension into frequency to give the space-frequency SVD. Below another application of the SVD is presented for extracting responses to periodically presented stimuli.

Space-time SVD

The space-time SVD is a one step operation on the space-time data $I(x, t)$. The SVD of such data is given by

$$I(x, t) = \sum_n \lambda_n I_n(x) a_n(t) \quad \text{Equation 6}$$

where $I_n(x)$ are the eigenmodes of the "spatial correlation matrix" $\int_{-\infty}^{\infty} I(x,t)I(x',t)dt$.

Similarly $a_n(t)$ are the eigenmodes of the "temporal correlation matrix"

$\int_{-\infty}^{\infty} I(x,t)I(x,t')dx$. The eigenvalues, λ_n , give the amount of power or variance in each of the ordered space and time eigenmodes. Their relative values give an indication of how large the signal is compared to the noise. Discarding modes with small eigenvalues allows a data dimension reduction for the purposes of visual inspection.

Applications of the SVD on space-time imaging and receptive field data are abundant in the literature: see (Golomb et al., 1994) for a didactic presentation. However, in our experience the SVD when applied to the space-time data suffers from a severe drawback because there is no reason why the neurobiologically distinct modes in the data should be orthogonal to each other. In practice this means segregation of the activity may be prevented because different sources of fluctuations may appear in a single mode of the decomposition or a single activity pattern may appear across different modes.

In the next section a more effective way of separating distinct components in the data using a decomposition analogous to the space-time SVD, but in the space-frequency domain. The success of the method stems from the fact that the data in question are better characterized by a frequency based representation.

Space-frequency SVD

The basic idea is to project the space-time data to a frequency interval, and then perform an SVD on this space-frequency data (Thomson and Chave, 1991; Mann and Park, 1994; Mitra et al., 1997). Projecting the data on a frequency interval can be performed effectively by using DPSS with the appropriate bandwidth parameter.

Step 1: Constructing the space-frequency matrix

Given the $N_x \times N$ space-time data matrix $I = I(x,t)$, the space-frequency data corresponding to the frequency band $[f - W, f + W]$ are given by the $N_x \times K$ matrix of complex numbers.

$$\tilde{I}(x,k;f) = \sum_{t=1}^N I(x,t)w_k(t,W)\exp(2\pi ift)$$

Equation 7

Step 2: SVD of the space-frequency matrix

We are considering the SVD of the $N_x \times K$ complex matrix with entries $\tilde{I}_n(x; f)$ for fixed f .

$$\tilde{I}_n(x; f) = \sum_n \lambda_n(f) \tilde{I}_n(x; f) a_n(k; f) \quad \text{Equation 8}$$

This SVD can be carried out as a function of the center frequency f , using an appropriate choice of W . At each frequency f one obtains a singular value spectrum $\lambda_n(f)$ ($n=1,2,\dots,K$), the corresponding (in general complex) spatial mode $\tilde{I}_n(x; f)$, and the corresponding local frequency modes $\tilde{a}_n(k; f)$. The interval W separates independent values of frequency in this analysis. The frequency modes can then be projected back into the time domain to give (narrowband) time-varying amplitudes of the complex eigenimage (Mann and Park, 1994).

Step 3: A measure of spatial coherence

In the space-frequency SVD computation, an overall coherence $\bar{C}(f)$ may be defined as (it is assumed that $K \leq N_x$)

$$\bar{C}(f) = \frac{\lambda_1^2}{\sum_{n=1}^K \lambda_n^2(f)} \quad \text{Equation 9}$$

The overall coherence spectrum then reflects how much of the fluctuation in the frequency band $[f - W, f + W]$ is captured by the dominant spatial mode. The value ranges between 0 and 1 and for random data $\bar{C}(f) \approx 1/K$. This sets a threshold for significance.

Periodic Signals, Trial Averaging and High-Resolution Methods

Experimental data of the dynamical response of a noisy system to a stimulus typically consist of repeated measurements of the response of the system to one or more stimuli. The most common method for increasing the signal-to-noise ratio for stimulus-response data is to average repeated measurements of the response, a method called trial-averaging. The methods described above can all be used with simple trial-averaging of responses. Improvements can, however, be made on simple trial averaging by using high-resolution sinusoid detection methods in the frequency domain that were presented above.

One approach that makes use of sinusoid detection methods in the frequency domain is called the *periodic stacking method* (Sornborger et al., 2003a). This method was developed to denoise and characterize the response to stimulus in optical imaging data of the intrinsic signal in cats and macaques. A related method has been used to characterize periodic electrical activity in the heart (Sornborger et al., 2003b). The technique is similar in spirit to that presented by Kalatsky and Stryker (2003), but involves extraction of stimulus information at all harmonics of the stimulus frequency, not just the fundamental. When the signal lies in a distinct band of frequencies, the signal-to-noise ratio of periodic stacking estimates significantly increases relative to the trial averaged estimate. Further improvements can be made in multivariate estimates, in which a subspace of the vector space within which the images lie can be identified as containing statistically significant signal.

The Periodic Stacking Method

We begin by considering univariate stimulus-response data. During an experiment, multiple responses to a stimulus are measured. We assume all response measurements $x_m(t)$ defined for $0 < t < T$ are of equal duration and concatenate all the M responses to a given stimulus. The resulting function, of duration MT , we denote by $X(t)$. We define $X(mT + t) \approx x_m(t)$ where $x_m(t)$ is the measured response to the m^{th} repetition of the stimulus, of duration T . Since we are measuring M responses to the same stimulus, the signal $X(t)$ is a combination of a T -periodic piece and measurement noise, ε .

$$X(t) = \sum_f \alpha_f \exp(2\pi i f t / T) + \varepsilon(t) \quad \text{Equation 10}$$

To understand the structure of the signal in Fourier space, we perform a Fourier transform on the signal

$$X(t) = \sum_q \tilde{x}_q \exp(2\pi i q t / MT) \quad \text{Equation 11}$$

The coefficients \tilde{x}_q are then given by the expression

$$\tilde{x}_q = \sum_f \alpha_f \delta(q - fM) + \tilde{\varepsilon}(q) \quad \text{Equation 12}$$

where $\tilde{\varepsilon}(q)$ indicates the Fourier transform of the noise, ε . From this expression, we see that the signal is a sequence of harmonics, α_f , at frequencies that are integral multiples of the base, stimulus frequency $2\pi/T$ (i.e. $q/M = f$).

We can estimate the signal from the frequency and complex amplitude of the harmonics that carry the response. We use multitaper harmonic analysis described above to accurately determine the amplitude and phase of the periodic response. This also gives an estimate of the noise and the statistical significance of deterministic sinusoids in a signal using equations 3,4 and 5. Since we know the periodicity of the repeated stimulus, we identify and extract the sinusoids in the data that lie at multiples of that base frequency. Response contributions that are not located at frequencies commensurate with the base frequency are discarded as noise. We then recombine the estimated sinusoids, to form an estimate of the response as before. This procedure is equivalent to demodulating the data at the stimulus frequency and harmonics of the stimulus frequency and summing the demodulates.

The periodic stacking method can be extended to the case of a multivariate dataset using the SVD. It is impractical to analyze a typical set of images pixel-by-pixel, due to the fact that there are often $P = 10,000$ pixels or more per image. So we first perform a singular value decomposition on the data, $I(x, t)$. Usually, most of the variance in the data is captured in the first 100 or 200 eigenfunctions. We can therefore consider the compressed dataset

$$I(x, t) = \sum_{n=1}^Q \lambda_n I_n(x) a_n(t) \quad \text{Equation 13}$$

where $Q = 200$, for example. With this step, we have thrown away $P-200$ eigenfunctions. However, we hope not to have thrown away the signal. One should always investigate as many eigenfunctions as possible for signal features, especially with unfamiliar data, so as to minimize the risk of throwing away signal in high index eigenfunctions.

The next step in the analysis is to use multitaper harmonic analysis, as described above, to estimate the amplitudes A_n for the time courses $a_n(t)$ at each harmonic of the stimulus frequency. For this application, the bandwidth of the estimate should be chosen to be slightly less than the stimulus frequency. This choice avoids any significant overlap that might introduce correlations between harmonic estimates.

Following the multitaper harmonic analysis procedure, we can obtain the estimates for sinusoidal components at each harmonic of the stimulus frequency. Then we check, harmonic by harmonic, to see if there are any statistically significant sinusoids in any of the first Q time series $a_n(t)$. As described above, statistical significance is determined by checking the value of the cumulative distribution function of the F-statistic for a given harmonic component is larger than $1 - 1/N$. We then assemble an estimate of the statistically significant periodic content:

$$\hat{I}(x, t) = \sum_{n=1}^Q \lambda_n I_n(x) \hat{a}_n(t)$$

Equation 14

where $\hat{a}_n(t)$ is the sum over statistically significant estimates for each harmonic of the stimulus frequency.

Estimates obtained using the multivariate signal estimation method outlined above have higher signal-to-noise ratios (SNR) than trial-averaged estimates largely because this method makes use of a measure of the statistical significance of the harmonics across all Q eigenfunctions $a_n(t)$. Therefore, eigenfunctions with no statistically significant content are discarded. Noise associated with these eigenfunctions is thereby eliminated, in contrast to trial-averaged estimates.

The above discussion is simplified as we only consider the case where a single repeated stimulus is presented to the animal. The intrinsic optical signal measures changes in reflectance of the cortex due to subtle changes in blood oxygenation. Responses to multiple stimuli in optical imaging measurements of the intrinsic signal typically consist of a change in the global blood oxygenation and blood volume that is not related to any particular stimulus (the *non-specific* response), accompanied by relatively smaller local changes in deoxy- and oxyhemoglobin concentrations that change depending on the stimulus (the *stimulus-specific* response). This approach can also be extended to distinguish between these two aspects of the signal (Sornborger et al., 2003c).

Protocol and procedures

Step 1: Visualization of the raw data

Direct visualization of the raw data is the first step to check the quality of the experiment and direct further analysis. Individual time series from the images and movies of the images should be examined. If the images are noisy, for example due to large shot noise, truncation of a space-time SVD with possibly some additional smoothing provides a simple noise reduction step for the visualization.

[Figure 1 approx. here]

A space-time SVD of the data is computed and the leading principal component time series modeled as a sum of sinusoids. This is useful for two reasons: (1) The images in question typically have many pixels, and it is impractical to perform the analysis separately on all pixels. (2) The leading SVD modes capture a large degree of global coherence in the oscillations. However, the procedure may as well be applied to individual image time series.

Step 2: Preliminary characterization

The next stage aims to identify the various artifacts and determine a preliminary characterization of the signal. A time-frequency spectral estimate described above should be calculated. This can be done on individual pixels or a space-time SVD can be first calculated followed by operations on the leading principal components.

[Figure 2 approx. here]

A more powerful characterization is obtained by the space-frequency SVD. There is sufficient frequency resolution in optical data so that, as a practical matter, the oscillatory artifacts tend to segregate well. Studying the overall coherence spectrum reveals the degree to which the images are dominated by the respective artifacts at the relevant frequencies, while the corresponding leading eigenimages show the spatial distribution of these artifacts more cleanly compared to the space-time SVD. Moreover, provided the stimulus response does not completely overlap the artifact frequencies, a characterization is also obtained of the spatio-temporal distribution of the stimulus response.

Step 3: Artifact removal

Based on the preliminary inspection stage, one can proceed to remove the various artifacts to the extent possible. The techniques described in this chapter are most relevant to artifacts that are sufficiently periodic, such as cardiac/respiratory artifacts, 50/60 Hz and other frequency-localized noise such as building or fan vibrations. An example of artifact removal from data from rat primary somatosensory cortex is presented below.

Step 4: Stimulus-response characterization

This may be the most delicate step, since the goal of the experiment is usually to find the stimulus response that is not known *a priori*. If the stimulus is presented periodically and/or repeatedly, as is usually the case, the characterization of stimulus response is fairly straightforward using the periodic stacking method. An example of this technique on data from cat visual cortex is presented below. Alternatively, coherent activity related to a single presentation of the stimulus may also be efficiently extracted by the space-frequency SVD technique if the stimulus response is known *a priori* to inhabit a particular frequency band (including a low frequency band). An example of the use of this technique may be found in (Prechtl et al., 1997).

Example of application

In this section we present an application of the tools described above to intrinsic signal optical imaging data. There are two stages to the analysis, exploratory and confirmatory. Exploratory analysis determines parameters of interest and the structure of any noise present. Following this, the noise is filtered and the signal structure characterized. The first application presents techniques for denoising intrinsic optical imaging data from rat

primary somatosensory cortex. The second application presents techniques for characterizing signal structure from intrinsic optical imaging data from cat primary visual cortex.

Application 1

Experimental method

Widefield fluorescent imaging was used to record optical signals from the surface of rat somatosensory cortex. The subjects were Sprague-Dawley rats prepared and maintained as described previously (Kleinfeld and Delaney, 1996). In brief, bone and dura were removed from a 4-by-4 mm region of the primary vibrissa areas of parietal cortex. The exposed cortex was then stained with the dye RH-795 (Molecular Probes, Eugene, OR). A metal frame was fixed to the skull that surrounded the craniotomy as a means to rigidly hold the head of the animal to the optical apparatus. With the addition of agarose gel and a cover glass window, this frame further served as an optically clear chamber that sealed and protected the cortex; resealing the craniotomy was crucial for the mechanical suppression of excessive motion that would otherwise result from changes in cranial pressure with each heart beat and breath.

We recorded the fluorescent yield from the cortical surface with a charge coupled device (CCD) camera (no. PXL 37; Photometrics, AZ). The signal was calculated as the change in fluorescence relative to the background level, i.e., $\Delta F = (I - I_{avg}) / I_{avg}$ where I_{avg} is the average intensity in the record. For the sample data shown in figure 1, the pixel field was 30 by 90, the sampling rate was 95.4 Hz, and records were 3000 frames (286 s) in length. Each digitized CCD pixel collected up to an estimated 300,000 electrons, so that the sensitivity per pixel per sample (or per frame) was limited to a fractional change of ~ 0.002 . The electrocardiogram, as an indicator of heart rate, and chest expansion, as an indicator of respiration, were further recorded. For the sample data shown in figure 1, no stimuli were applied to the rat during data acquisition.

We now consider practical issues involved in implementing harmonic analysis on our widefield imaging data. These considerations hold for both voltage sensitive dye images (Fig. 1a) as well as intrinsic optical imaging of rat somatosensory cortex. Prior to the harmonic analysis, we reduced the impact of artifacts associated with large blood vessels by excluding pixels inside such blood vessels from further analysis. The main harmonic artifacts in our datasets were due to breathing, heartbeat, mixing of the breathing and heartbeat, and a vibrational mode in the building.

As a first means to decrease processing time, we assumed that the dominant frequency of each harmonic artifact was independent of the spatial extent of the images. To identify the artifacts, we averaged all pixels in each image frame to generate a univariate time series and calculated the spectra from the entire time window. In practice, we selected a range of frequencies for each artifact by hand since the relevant frequencies may drift during the acquisition of the image series. In typical data sets, heartbeat, breathing and vibration artifact frequencies remained stable enough over several hours to use a fixed set

of frequency ranges. The selected frequency range were chosen to be wide enough that they covered the variations of the artifact, but narrow enough that only one harmonic artifact was present in each range.

We used sliding windows to detect and track changes in the amplitude of the artifact over time. These windows were typically 1.5 s long and were shifted by 0.1 s. The frequency for each artifact was fit at each point in time by calculating the direct multitaper spectral estimate in each sliding time window (Eqns. 1 to 4). We selected the frequency with the largest F-statistic within the user-selected artifact band to represent the dominant artifact frequency at that point in time (Fig. 1b). It is possible for several frequencies for one artifact in a time window to be significant according to the F-statistic test because the frequency of the artifact may shift, or because the frequency resolution of the spectral estimate is less than the Rayleigh range.

After the time course of artifact frequencies are identified, the phase and amplitude of the harmonic artifacts can be calculated for each pixel in the series of images. A direct approach is to treat each pixel in the image data as a time series that is used to calculate the phase and amplitude of each artifact at that point in space. This approach can be computationally intensive due to a large number of pixels. Alternatively, as our second procedure to decrease processing time, we use the space-time SVD to reduce the number of components that require harmonic analysis. In practice, a typical number of significant modes was determined empirically to be 0.1 of eigenmodes; for the present example with 3000 modes (Fig. 1a), about 300 independent time series would be analyzed. The harmonic analysis to determine phase and amplitude at the frequency of the artifacts was performed only on the SVD time eigenmodes associated with significant eigenvalues.

In both the pixel-by-pixel and the space-time SVD analysis, each harmonic artifact was modeled by using a sliding window in time. Finally, the reconstructed artifact was subtracted from the original time series (Percival and Walden, 1993). For the space-time SVD analysis, the artifact-free time eigenmodes and their corresponding eigenvalues and space eigenmodes were used to calculate a new series of images.

Application 2

Experimental method

The experiments were carried out on adult (2-5 kg) cats (*Felis domestica*). Anesthesia was induced with intramuscular injections of Xylazine [Rompun (Miles), $2 \text{ mg}\cdot\text{kg}^{-1}$] and Ketamine [Ketaset (Fort Dodge Laboratories, Fort Dodge, IA), $10 \text{ mg}\cdot\text{kg}^{-1}$] and later was maintained with intravenous (i.v.) infusion of Pentothal (Astra, Westborough, MA) ($1\text{-}3 \text{ mg}\cdot\text{kg}^{-1}\cdot\text{hr}^{-1}$). Muscular paralysis was induced by i.v. infusion of Pancuronium bromide (Abbott) ($1.3 \text{ mg}\cdot\text{kg}^{-1}\cdot\text{hr}^{-1}$). The state of anesthesia was monitored and maintained carefully in accordance with the National Institutes of Health guidelines. The animals

were respired mechanically and the end-expiratory concentration of CO₂ was kept at 3.5-4%. Blood pressure, electroencephalogram, electrocardiogram, and core body temperature were monitored and maintained within normal physiological ranges. A craniotomy and durotomy exposed a region of V1 cortex corresponding to 2-8° eccentricity in the visuotopic representation. A cylindrical, stainless steel, glass-topped chamber was attached to the skull with screws and plumbers epoxy (Propoxy 20, Hercules, Passaic, NJ), and was filled with inert silicone oil. The cortex was illuminated uniformly with 600 nm light and imaged through a tandem-lens configuration by using a cooled 12-bit charge-coupled device (PXL, Photometrics, 536 × 389 pixels) that was synchronized to the cardiac and respiratory cycles.

An example of results using the periodic stacking method is shown in Figure 3. In panels A and C, we plot the first two eigenfunctions resulting from an SVD of the estimated signal $\hat{I}(x, t)$. In panels B and D we plot estimates of their time courses plotted with one-sigma (i.e. one standard deviation of the standard error of the mean) error bars. The vertical lines denote changing stimulus. The first segment is the response to a 0° oriented drifting grating, the second is the response to a 30° oriented drifting grating, etc. These two eigenfunctions make up 95% of the estimated signal.

[Figure 3 approx here]

The eigenfunction in A is responsible for most of the signal at 0° and 90°, while the eigenfunction in C is responsible for most of the signal at 45° and 135°. The envelopes of the responses of these two eigenfunctions form a cosine and sine. This is due to the periodic nature of the stimulus (rotate the orientation of a drifting grating by 180° and the grating is back at 0°) The spatial dapppling of the eigenfunctions gives rise to the classic result (Blasdel, 1992a, 1992b; Everson et al., 1998) that singularities or pinwheels exist in the response to oriented drifting grating stimuli. As the orientation of the drifting grating changes, the maximum response rotates about the pinwheels. Note that the sharp changes in dynamics in the signal at the boundaries between the changing stimuli are accurately captured. These changes are introduced artificially when the data were concatenated.

Advantages and limits

Spectral methods, with averaging of selected frequency bands, rejection of physiological artifacts, and statistical tests of significance, provide a robust means to analyze imaging data with significant correlations in space and time. For example, the raw data of Figure 3 had a signal-to-noise ratio of 0.0002 which was increased to 21 after processing. The ability to compute confidence limits on the results of the analysis provides a means to compare and contrast features across time and across different data sets. The main limitation of this approach is that in general, when no model for signal is proposed the resolution of the estimates is limited because the time-bandwidth product must be greater than 1.

Acknowledgements

The authors thank L. Sirovich and T. Yokoo for their collaboration and C. Sailstad for the use of her optical imaging data. This work was supported by grants from the NCR (RR13419 to DK) and NINDS (NS41096 to DK) and a NSF predoctoral fellowship to NN. Many of the techniques described here were devised or refined as part of the NIMH sponsored “Workshop on the Analysis of Neural Data” at the Marine Biological Laboratories.

References

- Blasdel GG (1992a) Differential imaging of ocular dominance and orientation selectivity in monkey striate cortex. *J Neurosci* 12:3115-3138.
- Blasdel GG (1992b) Orientation selectivity, preference, and continuity in monkey striate cortex. *J Neurosci* 12:3139-3161.
- Everson RM, Prashanth AK, Gabbay M, Knight BW, Sirovich L, Kaplan E (1998) Representation of spatial frequency and orientation in the visual cortex. *Proc Natl Acad Sci U S A* 95:8334-8338.
- Golomb D, Kleinfeld D, Reid RC, Shapley RM, Shariman BI (1994) On temporal codes and the spatiotemporal response of neurons in the lateral geniculate nucleus. *J Neurophysiol* 72:2990-3003.
- Kalatsky VA, Stryker MP (2003) New paradigm for optical imaging: Temporally encoded maps of intrinsic signal. *Neuron* 38:529-545.
- Kleinfeld D, Delaney K (1996) Distributed representation of vibrissa movement in the upper layers of somatosensory cortex revealed with voltage sensitive dyes. *J CompNeurol* 375:89-108.
- Mann ME, Park J (1994) Global-scale modes of surface temperature. *J Geophys Res Atmos* 99:25819-25833.
- Mayhew JE, Askew S, Zheng Y, Porrill J, Westby G, Redgrave P, Rector D, Harper R (1996) Cerebral vasomotion: 0.1 Hz oscillation in reflected light imaging of neural activity. *Neuroimage* 4:183-193.
- Mitra PP, Pesaran B (1999) Analysis of dynamic brain imaging data. *Biophys J* 76:691-708.
- Mitra PP, Ogawa S, Hu XP, Ugurbil K (1997) The nature of spatiotemporal changes in cerebral hemodynamics as manifested in functional magnetic resonance imaging. *Magn Reson Med* 37:511-518.
- Percival DB, Walden AT (1993) Spectral analysis for physical applications. Cambridge: Cambridge University Press.
- Prechtl J, Cohen LB, Pesaran B, Mitra PP, Kleinfeld D (1997) Visual stimuli induce waves of electrical activity in turtle cortex. *Proc Natl Acad Sci U S A* 91:12467-12471.
- Sornborger A, Sirovich L, Morley G (2003b) Extraction of periodic multivariate signals: Mapping of voltage-dependent dye fluorescence in mouse heart. *IEEE Trans Med Imag* In press.
- Sornborger A, Sailstad C, Kaplan E, Knight B, Sirovich L (2003a) Spatio-temporal analysis of optical imaging data. *Neuroimage* 18:610-621.

- Sornborger A, Delorme A, Sailstad C, Kaplan E, Sirovich L (2003c) Extraction of the average and differential dynamical response in stimulus-locked experimental data. Submitted to Neuroimage.
- Thomson DJ (1982) Spectrum estimation and harmonic analysis. Proc IEEE 70:1055-1996.
- Thomson DJ, Chave AD (1991) Jackknifed error estimates for spectra, coherences, and transfer functions. In: Advances in Spectrum Analysis and Array Processing, pp 58-113. Englewood Cliffs, NJ: Prentice Hall.

Figure Captions

Figure 1: Optical imaging data from rat somatosensory cortex.

- a) Noise suppression of cardiac and respiratory rhythms. The figure shows the results of filtering the respiratory and cardiac rhythms from a single principal component mode in the time domain. The top curve is the raw mode. The middle curve shows the reconstructed noise signal using the overlap-add technique described in the text. The bottom curve shows the residual signal after noise suppression.
- b) Time-frequency representation of the raw mode from the top of a). The black lines show the estimated frequency tracks. The fundamental of the respiratory rhythm was at 1.5Hz and that of the cardiac rhythm at 7Hz.

Figure 2: Space-Frequency SVD.

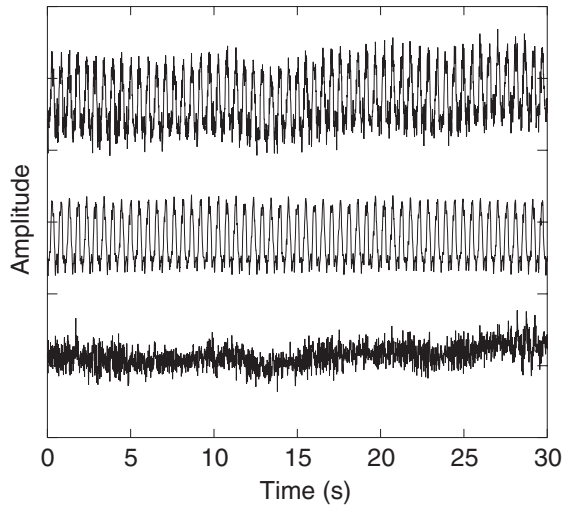
- a) The amplitude of the dominant eigenimages as function of center frequency. The respiratory rhythm is present as a derivative highlighting the blood vessels at 2Hz and harmonics. The cardiac rhythm is present as an increase in luminescence on the vessel at 6.8Hz. At intermediate frequencies spatial structure is diminished.
- c) Overall coherence for the eigenimages in a).

Figure 3: Results from a periodic stacking estimate of the stimulus-specific response of cat primary visual cortex to oriented drifting grating stimuli at 0° , 30° , ..., 150° .

- a,c) The first two eigenfunctions of a singular value decomposition of the estimated signal $\hat{I}(x, t)$.
- b,d) Estimates of the time courses plotted with one-sigma (i.e. one standard deviation of the standard error of the mean) error bars. See text for discussion.

Figure 1

a)



b)

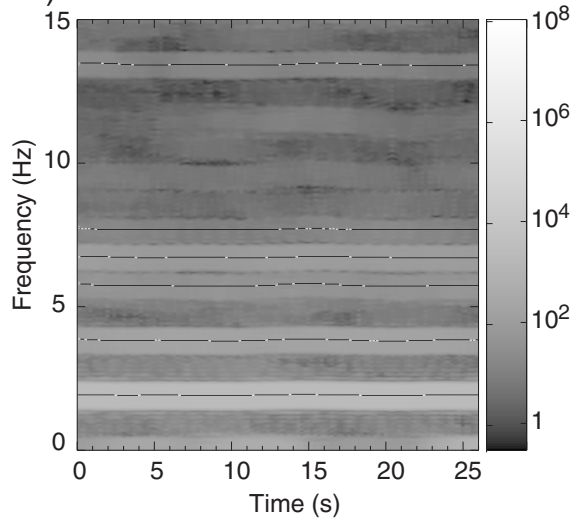
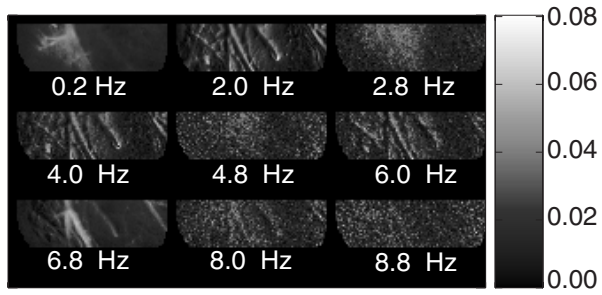


Figure 2

a)



b)

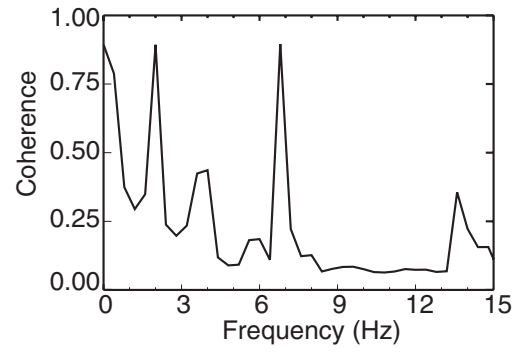
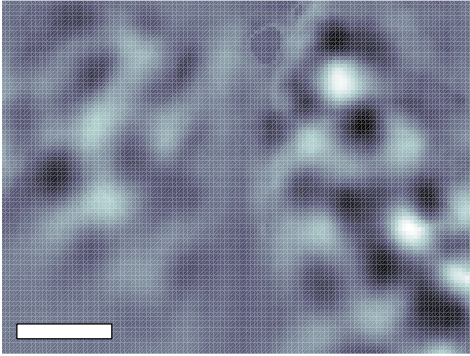
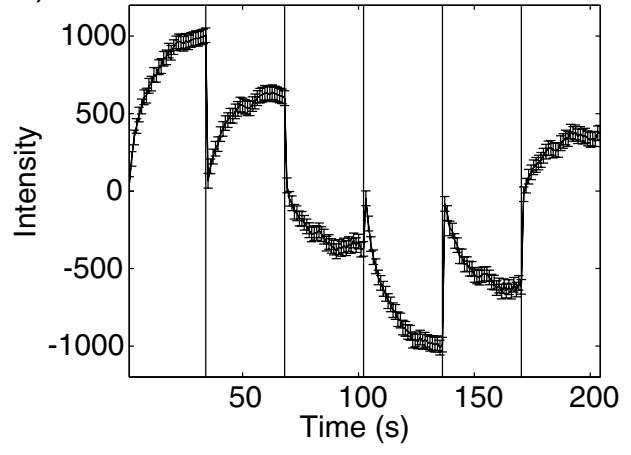


Figure 3

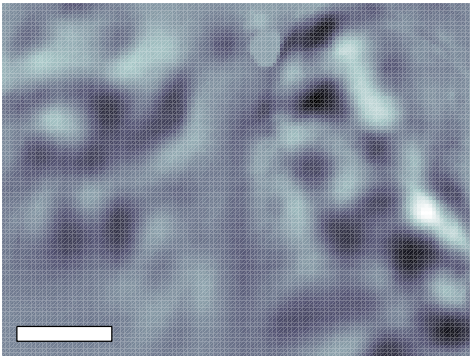
a)



b)



c)



d)

